# Supplement 1

# High performance multimode fiber specklegram sensing with multi-layer convolutional neural network based on digital aperture filtering

### Supplementary section 1: Performance comparison with deep learning-based FSS

In the existing literatures, many studies have demonstrated the potential of machine learning algorithms in processing speckle patterns and achieving precise sensing. For instance, Smith et al. utilized two deep neural networks to measure air temperature and water immersion length [1]. Song et al. extracted feature information from speckle patterns using deep learning to estimate both the bending direction and curvature [2]. Mostafavi et al. employed a CNN model to learn the relationship between fiber deformation parameters and changes in the shape and structure of speckle patterns, achieving measurement of the deflection direction at the tip of a multimode fiber [3]. Liu et al. used a deep learning regression model to implement a fiber curvature sensor based on the detection of speckle patterns on the surface of a multimode fiber [4]. Additionally, Liu et al. established a relationship between the change process of speckle patterns and the torsion angle of MMF using a ResNet [5]. While these studies have achieved precise sensing of measurands in specific applications, they generally rely heavily on machine learning algorithms themselves and lack in-depth analysis of physical phenomena. As a result, their sensing capabilities may lack universality when the fiber is changed. As the number of modes supported by the fiber increases, the decorrelation speed becomes faster, leading to poorer sensing performance [5]. Therefore, these methods lack universality across different MMFs.

In addition, some studies such as Hu et al. have utilized a hybrid framework constructed with Principal Component Analysis (PCA) and Backpropagation (BP) neural networks. They employed the PCA algorithm to perform dimensionality reduction on the collected samples, eliminating redundant information and noise [6]. Liu et al. used the Uniform Local Binary Pattern (ULBP) algorithm to extract texture feature vectors from each speckle image. Subsequently, a 1D CNN was utilized to map the texture feature vectors to the target curvature in a nonlinear manner [7]. While dimensionality reduction processing has enhanced the model's generalizability, these studies also lack in-depth analysis of the physical phenomena and do not fully explain the rationale behind the choice of specific algorithms and their working principles.

Song et al. proposed a deep learning-based flexible fiber sensor that leverages a deep optical neural network trained on a small dataset. The optical classification model, trained to classify speckle data under perturbed conditions, achieved an accuracy rate as high as 98.3% [8]. However, this resistance to interference is due to the introduction of artificial external interference sources during the collection of speckle data, and the use of deep learning to classify speckles under noisy conditions. Thus, this method relies more on the powerful learning capabilities of deep learning, with a lack of support from physical principles.

In summary, many current deep learning-based FSSs rely heavily on machine learning algorithms to process speckle patterns, often overemphasizing sensing accuracy rather than discussing the underlying physical phenomena. To address this shortcoming, our research introduces an innovative method known as the digital aperture filtering (DAF), which is an effective physical principle analysis supported by the incorporated deep learning techniques as

the data processing tool. We have thoroughly discussed the working principles of the DAF method, including how to utilize the differences in the energy density distribution characteristics between modes and how to select the optimal filtering parameters based on the physical properties of speckles. By integrating the deep learning technology, we have achieved high sensing performance of measurands. In the manuscript, we have conducted a comprehensive comparison between the DAF method and the traditional, deep learning-only, unfiltered speckle demodulation (uFSD) method. The results demonstrate that the DAF method shows significant advantages in both sensing accuracy, sensing range, stability, resolution, and generalizability.

Of course, we also need to point out that the limitation of our research lies in the insufficient ability to resist interference from the external environment, which is also a common challenge faced by FSS. To enhance the model's resistance to interference, we adopted the method of collecting data multiple times to increase sample diversity. This strategy is only suitable for minor disturbances; when the environment in which the fiber is located undergoes significant changes or extreme conditions, relying solely on increasing the number of data collections may not be enough to ensure the performance of the sensor. In these cases, further technological innovation and methodological improvements might be necessary, which will be a key focus of our future research.

## Supplementary section 2: The steps to obtain the correlation coefficient

The steps to obtain the correlation coefficient are as follows:

1. **Determination of the Reference Speckle Pattern:**
   For MMF 1 and MMF 2, the detection range of the light field direction is from -13° to 13°. Therefore, we selecte the speckle pattern collected at the incident light field direction of $\theta$ = -13° as the reference speckle pattern, denoted as $P$.
   For FMF 1, the detection range of the light field direction is from -6° to 6°. Consequently, the reference speckle pattern is set corresponding to the incident light field direction of $\theta$ = -6°.
2. **Speckle Pattern Collection:** Subsequently, we alter the incident light field direction by increments of angular displacement $\Delta\theta = 0.1°$ and record the speckle patterns at each angle, denoted as $I^{0.1}$, $I^{0.2}$, $I^{0.3}$, …, $I^{n}$. At each light field direction, 30 sets of speckle patterns are collected.
3. **Calculation of the Correlation Coefficient:** For each set of collected speckle patterns $I^{n}$, the correlation coefficient $C\left(I^{n},P\right)$ with respect to the reference pattern $P$ can be expressed as:

$$C\left(I^{n},P\right)=\frac{\sum_{i=1}^{m}\left(I_i^n-\bar{I}^n\right)\left(P_i-\bar{P}\right)}{\sqrt{\sum_{i=1}^{m}\left(I_i^n-\bar{I}^n\right)^2\sum_{i=1}^{m}\left(P_i-\bar{P}\right)^2}} \tag{S1}$$

where, $I_i^n$ and $P_i$ are the intensity values of corresponding pixels in the two speckle patterns. $\bar{I}^n$ and $\bar{P}$ are the mean values of the two speckle patterns. $m$ is the total number of pixels in the speckle patterns. $C\left(I^{n},P\right)$ is the correlation coefficient between the two speckle patterns, which ranges from -1 to 1, where 1 indicates a perfect positive correlation, -1 indicates a perfect negative correlation, and 0 indicates no linear correlation. By averaging the correlation coefficients of the 30 sets of data, the comprehensive correlation coefficient for each light field direction is obtained.

4. **Analysis of the Correlation Coefficient:** The calculated correlation coefficients are plotted as a curve, and the trend of their variation with the change in the light field direction is observed.

## Supplementary section 3: The steps to determine the optimal DAFR

The process for determining the optimal DAFR:

1. **Theoretical Foundation:** Liu et al. [5, 7] pointed out in their research that the smaller the decorrelation angle of the speckle, the lower the sensing accuracy for measurands. Therefore, our goal is to find the DAFR value that can produce the largest decorrelation angle.
2. **Preliminary Screening:** Initially, we represent the core radius as "$a$" and calculate the speckle correlation coefficients for DAFR at decrements of $a/1$, $a/2$, $a/3$, ..., $a/6$, which can help us to determine the approximate range of the optimal DAFR.
3. **Fine-tuning:** Based on the preliminary screening, we find that the speckles of MMF 1 and MMF 2 have the largest decorrelation angles when the $R = a/3$. To further refine the optimal DAFR, we calculate the DAFR values at a step size of 0.1 around $a/3$, specifically at $a/2.5$, $a/2.6$, $a/2.7$, ..., $a/3.5$.
4. **Final Determination:** By comparing the speckle correlation coefficients and decorrelation angles corresponding to these more closely step size DAFR values, we determine the optimal DAFR for MMF 1 to be $R = a/2.7$, and for MMF 2, the optimal DAFR is $R = a/3$.

## Supplementary section 4: The MLCNN training parameters

In the MLCNN training, mean squared error (MSE) serves as the loss function, and Stochastic Gradient Descent (SGD) is the optimizer. The initial learning rate is set to 0.004, and a dynamic learning rate adjustment strategy is adopted, reducing the learning rate by half every five training epochs to effectively mitigate overfitting. Additionally, to eliminate any potential dependency on the order of the training data, we randomly shuffle the dataset at the start of each training epoch, further reducing the possibility of overfitting.

## Supplementary section 5: MLCNN dataset composition

For MMF 1 and MMF 2, the incident light field direction $\theta$ is adjusted with a step size of 0.1°, ranging from -13° to 13°, a total of 261 light field directions, with 50 images collected for each direction. The data are divided into the training and validation sets with a 4:1 ratio, comprising 10,450 and 2,600 speckle images, respectively. The test data is further divided into Test set I and Test set II, with the incident light field direction $\theta$ adjusted with 0.5° step size. For each light field direction, 30 speckle images are collected. Test set I covers 53 directions ranging from -13° to 13°, comprising a total of 1,590 images. Test set II covers 52 directions ranging from -12.75° to 12.75°, comprising a total of 1,560 images.

For FMF 1, we employ a similar data collection method, but the range of the incident light field direction $\theta$ is from -6° to 6°, a total of 121 directions, with 50 images captured for each direction. The data are divided into a training set and a test set, consisting of 4,850 and 1,200 speckle images, respectively. Test set I covers 25 directions ranging from -6° to 6°, comprising a total of 750 images. Test set II covers 52 directions ranging from -5.75° to 5.75°, comprising a total of 720 images. The sizes of the MLCNN's datasets corresponding to different fibers are shown in Table S1.

**Table S1. The sizes of the MLCNN's datasets corresponding to different fibers.**

| | Number of training set | Number of validation set | Number of Test set I | Number of Test set II |
|---|---|---|---|---|
| MMF 1 | 10450 | 2600 | 1590 | 1560 |
| MMF 2 | 10450 | 2600 | 1590 | 1560 |
| FMF 1 | 4850 | 1200 | 750 | 720 |

## Supplementary section 6: Sensing performance evaluation

We have conducted a thorough comparison in terms of sensing accuracy, sensing range, stability, resolution, and generalizability.

**Sensing Accuracy:** We use the mean absolute error (MAE) as the benchmark for assessing sensing accuracy. For the light field direction sensing results of different fibers and methods presented in Table 1, we have calculated the MAE for both the DAF method and the uFSD method. The reduction in MAE achieved by employing the DAF method over the uFSD method is calculated using the following equation:

$$Reduction\ in\ MAE = \left(1 - MAE_{DAF} / MAE_{uFSD}\right) \times 100\% \tag{S1}$$

where, $MAE_{DAF}$ is the mean absolute error when using the DAF method, $MAE_{uFSD}$ is the mean absolute error when using the uFSD method.

Based on the calculations, for MMF 1, the sensing error in Test set I using the DAF method is reduced by 53% compared to the uFSD method, and the sensing error in Test set II is reduced by 56%. For MMF 2, the sensing error in Test set I is reduced by 44% with the DAF method, and the sensing error in Test set II is reduced by 49%. Combining the results from both test sets, it is evident that the sensing error using the DAF method has been significantly reduced across different test conditions. On average, the MAE is 50% lower than the MAE of the uFSD method, a statistic that strongly indicates the significant advantage of the proposed DAF method in terms of sensing accuracy.

**Sensing Range:** According to the light field direction sensing results of MMF 1 and MMF 2 in Fig. 4 and Fig. 5, it can be seen that the uFSD method exhibits larger sensing errors when dealing with large angle incident light fields ($\theta$ = -13° to -4°, and 4° to 13°), while it demonstrates higher sensing accuracy for small angle incidence ($\theta$ = -4° to 4°). By applying the DAF method to preprocess the speckle patterns, the errors in sensing large angle light field directions are effectively reduced. Therefore, the proposed DAF method not only maintains high precision in the small angle range but also significantly improves sensing capabilities in the large angle range, indicating a clear advantage of DAF method in expanding the sensing range.

**Stability:** We use the standard deviation (S.D.) to assess the stability of the sensing results of the light field direction. According to the S.D. of light field direction sensing results of different methods in Table 1, the reduction in S.D. achieved by using the DAF method compared to the uFSD method can be calculated using the following equation:

$$Reduction\ in\ S.D. = \left(1 - S.D._{DAF} / S.D._{uFSD}\right) \times 100\% \tag{S2}$$

where, $S.D._{DAF}$ is the standard deviation when using the DAF method, $S.D._{uFSD}$ is the standard deviation when using the uFSD method.

For MMF 1, the S.D. of Test set I based on the DAF method is reduced by 55% compared to the uFSD method, and the S.D. of Test set II is reduced by 66%. For MMF 2, the S.D. of Test set I based on the DAF method is reduced by 47% compared to the uFSD method, and the S.D. of Test set II is reduced by 50%. Combining the results from both test sets, we observe that the S.D. based on the DAF method is approximately 55% lower than the uFSD method, indicating that our method has a significant advantage in terms of stability.

**Resolution:** We employ the $3\sigma$ rule to the evaluation of the sensor's resolution. Taking Test set Il as an example, we plot the distribution of absolute errors in the light field direction sensing results under different methods and calculate the distribution probabilities across various intervals based on the data's distribution characteristics, as illustrated in Fig. S1. Through these distributions, we can determine the error ranges at different confidence levels. Specifically, to meet the expectation that 99.7% of the absolute error values fall within the range of the mean value, for MMF 1, the resolution calculated based on the DAF method adopts the $\mu \pm 3\sigma$ relationship, while the uFSD method requires adopting the $\mu \pm 3.5\sigma$ relationship. For MMF 2,

the resolution calculated based on the DAF method adopts the $\mu \pm 4\sigma$ relationship, while the uFSD method requires adopting the $\mu \pm 4.5\sigma$ relationship. Where, $\mu$ represents the mean value of the absolute errors, which is the mean absolute error (MAE), and $\sigma$ represents the standard deviation (S.D.).

Using the MAE and S.D. of the light field direction sensing results provided in Table 1 for each method, we estimate the following resolution values:

For MMF 1, the light field direction resolution based on the DAF method is approximately 0.085°, while the resolution based on the uFSD method is approximately 0.274°. For MMF 2, the light field direction resolution based on the DAF method is approximately 0.335°, while the resolution based on the uFSD method is approximately 0.742°. From our experimental results, no matter it is MMF 1 or MMF 2, the resolution using the DAF method is superior to that of the uFSD method, and its resolution value is reduced by about 62%, indicating the advantage of our method in terms of sensor resolution.

**Generalizability:** We assess the generalization capability of our proposed DAF method using a Test set II that consists of data completely different from both the training set and Test set I [7]. Firstly, the sensing accuracy of Test set II is compared, and it is found that the sensing error of light field direction based on DAF is lower than that of uFSD. Furthermore, for MMF 1, the sensing error of Test set II based on the DAF method is 2.43 times that of Test set I, while the error based on the uFSD method is 2.58 times that of Test set I. For MMF 2, the sensing error of Test set II based on the DAF method is 3.80 times that of Test set I, while the error based on the uFSD method is 4.18 times that of Test set I. The results indicate that the gap in sensing errors between the two test sets based on the DAF method is smaller than that of the uFSD method, demonstrating that our DAF method exhibits better consistency and generalizability across different datasets.

Evaluating by the sensing accuracy, sensing range, stability, resolution, and generalizability, the proposed DAF method demonstrates superior performance over the traditional deep learning-based uFSD method in every aspect. This advantage stems from the design philosophy of the DAF method, which integrates physical principle analysis, takes into account the distribution characteristics of higher-order modes, and effectively reduces their influence through digital aperture filtering, thereby significantly enhancing the overall sensing performance of FSSs.

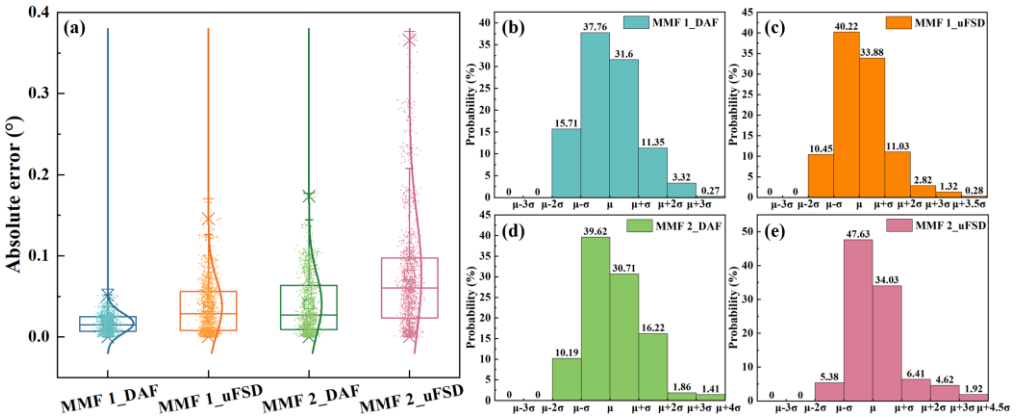


Fig. S1. (a) The distribution of absolute errors in the light field direction sensing results under different methods; The distribution probabilities of the absolute errors in the light field direction sensing results for different methods across various intervals are as follows: (b) MMF 1 with DAF method, (c) MMF 1 with uFSD method, (d) MMF 2 with DAF method, (e) MMF 2 with uFSD method. In the figure, $\mu$ and $\sigma$ represent the MAE and S.D., respectively, for the light field direction of the corresponding method.

## Supplementary section 7: Verification of the correctness of the optimal DAFR selection

To validate the correctness of the optimal DAFR selection for the speckles of MMF 1 and MMF 2, the sensing results of the light field direction based on DAF method are calculated at various DAFRs, as shown in Fig. S2. This is because the influence of higher-order modes is mainly screened out at the beginning, enhancing the correlation of speckles and increasing the decorrelation angle. At this stage, the speckles still retain effective feature information, so when MLCNN is used to train the filtered speckles, the sensing performance for the light field direction improves. However, as the DAFR is further reducing, the lower-order modes become dominant, the effective feature information of the speckles decreases, and the correlation among speckles is excessively enhanced, leading to a reduction in the decorrelation angle. This excessive correlation affects the ability of deep learning to recognize the rule of speckle changes under different light field directions, thereby increasing the sensing error. The results indicate that as the DAFR decreases, the sensing error first decreases and then increases. For MMF 1, the minimum sensing error occurs when the DAFR is $R$=62.5/(2*2.7) $\mu m$. For MMF 2, the minimum sensing error occurs at the DAFR is $R$=105/(2*3) $\mu m$. The DAFR corresponding to the minimum sensing errors are consistent with those that produce the maximum decorrelation angles, which indicates that our strategy of selecting the optimal DAFR based on the maximum decorrelation angle is scientifically sound and correct.

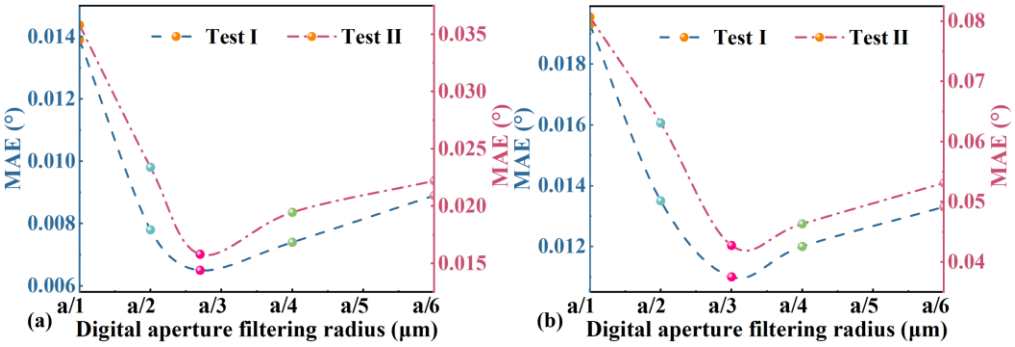


Fig. S2. The sensing results of the light field direction based on the DAF method at various DAFRs. (a) MMF 1; (b) MMF 2.

## Supplementary section 8: The impact of the number of convolutional layers on MLCNN performance

In the field of deep learning, the number of convolutional layers directly affects the model's learning capability and complexity. Adding convolutional layers can enhance the model's ability to capture complex features, but it may also increase the risk of overfitting and computational costs. To explore the impact of the number of convolutional layers on the performance of light field direction sensing, we have increased the number of convolutional layers based on the MLCNN used in the manuscript, and designate the new model as MLCNN-16. The sensing results of light field direction based on MLCNN-16 model under different DAFR are shown in Fig. S3.

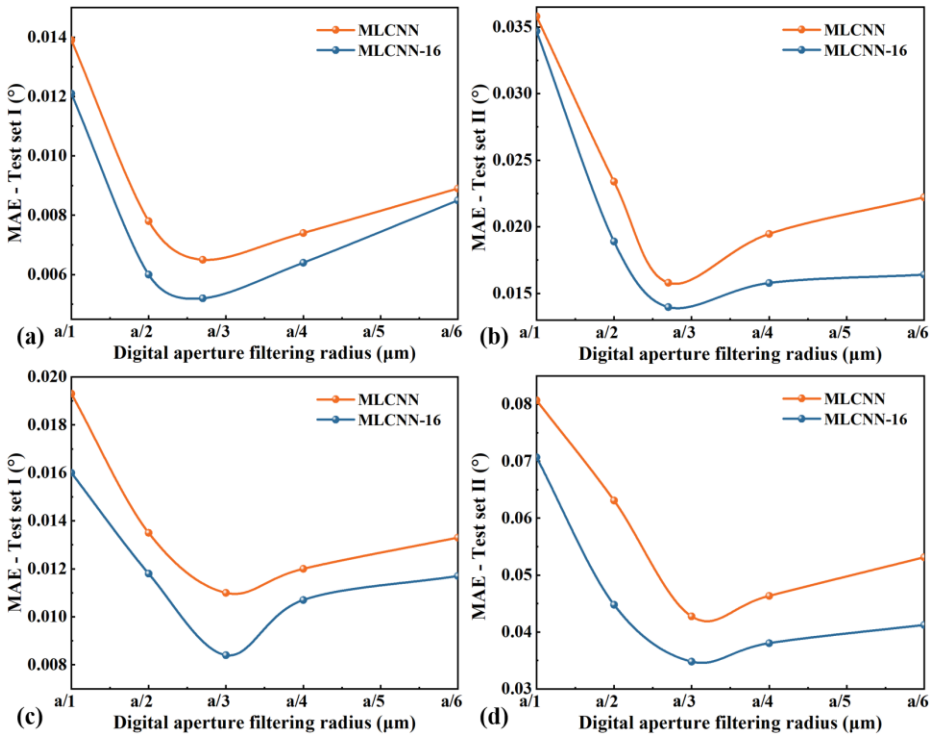


Fig. S3. The sensing results of the light field direction based on MLCNN-16 at various DAFRs. (a), (b) MMF 1; (c), (d) MMF 2.

From the figure, it can be observed that increasing the number of convolutional layers improves the sensing accuracy of the light field direction. However, the variation trend of the sensing results with DAFR is consistent with that of the MLCNN in the manuscript, where the DAFR corresponding to the minimum sensing error coincides with that corresponding to the maximum decorrelation angle. It is important to emphasize that the number of convolutional layers is not the more the better, an excessively deep network may lead to gradient disappearance or explosion problems, affecting the training stability of the model.

## References


1. T. D. Cabral, E. Fujiwara, S. C. Warren-Smith, H. Ebendorff-Heidepriem, and C. M. B. Cordeiro, "Multimode exposed core fiber specklegram sensor," Opt. Lett. **45**, 3212-3215 (2020).
2. X. Wang, Y. Yang, S. Li, X. Wang, P. Zhang, S. Lu, D. Yu, Y. Zheng, L. Song, and F. Fang, "A reflective multimode fiber vector bending sensor based on specklegram," Opt. Laser Technol. **170**, 110235 (2024).
3. S. Razmyar and M. T. Mostafavi, "Deep Learning for Estimating Deflection Direction of a Multimode Fiber From Specklegram," J. Lightwave Technol. **39**, 1850-1857 (2021).
4. G. Li, Y. Liu, Q. Qin, X. Zou, M. Wang, and F. Yan, "Deep learning based optical curvature sensor through specklegram detection of multimode fiber," Opt. Laser Technol. **149**, 107873 (2022).
5. G. Li, Y. Liu, Q. Qin, L. Pang, W. Ren, J. Wei, and M. Wang, "Fiber specklegram torsion sensor based on residual network," Opt. Fiber Technol. **80**, 103446 (2023).
6. H. Gao and H. Hu, "Spatially-resolved bending recognition based on a learning-empowered fiber specklegram sensor," Opt. Express **31**, 7671-7683 (2023).
7. G. Li, Y. Liu, Q. Qin, X. Zou, M. Wang, and W. Ren, "Feature Extraction Enabled Deep Learning From Specklegram for Optical Fiber Curvature Sensing," IEEE Sens. J. **22**, 15974-15984 (2022).
8. X. Gao, Y. Li, J. Wu, B. Song, H. Liu, X. Liu, and H. Sun, "Deep learning for highly efficient curvature recognition using fiber scattering speckles," Results Phys. **52**, 106808 (2023).